Three-Dimensional Structure of Butyryl-CoA Dehydrogenase from *Megasphaera elsdenii*[†,‡]

Snezana Djordjevic,[§] Charles P. Pace,[∥] Marian T. Stankovich,[∥] and Jung-Ja P. Kim*[,§]

Department of Biochemistry, Medical College of Wisconsin, Milwaukee, Wisconsin 53226, and Department of Chemistry, University of Minnesota, Minneapolis, Minnesota 55455

Received August 11, 1994; Revised Manuscript Received December 7, 1994[⊗]

ABSTRACT: The crystal structure of butyryl-CoA dehydrogenase (BCAD) from *Megasphaera elsdenii* complexed with acetoacetyl-CoA has been solved at 2.5 Å resolution. The enzyme crystallizes in the *P*422 space group with cell dimensions $a = b = 107.76$ Å and $c = 153.67$ Å. BCAD is a bacterial analog of short chain acyl-CoA dehydrogenase from mammalian mitochondria. Mammalian acyl-CoA dehydrogenases are flavin adenine dinucleotide (FAD)-containing enzymes that catalyze the first step in the β-oxidation of fatty acids. Although specific for substrate chain lengths, they exhibit high sequence homology. The structure of BCAD was solved by the molecular replacement method using the atomic coordinates of pig liver medium chain acyl-CoA dehydrogenase (MCAD). The structure was refined to an *R*-factor of 19.3%. The overall polypeptide fold of BCAD is similar to that of MCAD. E367 in BCAD is at the same position and in a similar conformation as the catalytic base in MCAD, E376. The main enzymatic differences between BCAD and MCAD are their substrate specificities and the significant oxygen reactivity exhibited by BCAD but not by MCAD. The substrate binding cavity of BCAD is relatively shallow compared to that of MCAD, as consequences of both a single amino acid insertion and differences in the side chains of the helices that make the binding site. The *si*-face of the FAD in BCAD is more exposed to solvent than that in MCAD. Therefore solvation can stabilize the superoxide anion and considerably increase the rate of oxidation of reduced flavin in the bacterial enzyme.

Megasphaera elsdenii, a Gram-negative anaerobe, ferments glucose, fructose, lactate, and other simple carbon compounds (Elsden & Lewis, 1953), producing an excess of reduced species. The organism eliminates this excess of reducing equivalents using short chain fatty acyl-CoA as the terminal electron acceptor. FAD-containing butyryl-CoA dehydrogenase (BCAD)[1] is a key enzyme in this reduction process. Although *in vivo* BCAD acts as a reductase, *in vitro* this enzyme is very similar to the mammalian acyl-CoA dehydrogenases that catalyze the first step in mitochondrial β-oxidation of fatty acids. *In vitro* BCAD catalyzes the oxidation of saturated acyl-CoA thioesters by removal of the two *pro-R*-hydrogen atoms. Characterization of the partially purified enzyme showed that, like mammalian acyl-CoA dehydrogenases, the enzyme requires electron-transfer flavoprotein (Baldwin & Milligan, 1964). BCAD is a tetramer with molecular mass of about 175 kDa with one molecule of FAD noncovalently bound per subunit. As isolated from *M. elsdenii*, BCAD exhibits a bright green color from a strong absorption band at 710 nm due to tightly bound CoA persulfide. This green color is also characteristic of mammalian short chain acyl-CoA dehydrogenases from ox, pig, and monkey liver (Mahler, 1954; Steyn-Parve & Beinert, 1958; Hoskins, 1966). The tightly bound CoA persulfide can be removed from the purified protein yielding a yellow form of the enzyme (Williamson & Engel, 1982).

Three mammalian soluble straight chain acyl-CoA dehydrogenases have been identified and classified on the basis of their distinct but overlapping substrate specificities for long, medium, and short chain fatty acids (Beinert, 1963). The amino acid sequence of BCAD (Becker et al., 1993) exhibits about 40% and 44% identities to those of medium (MCAD) and short (SCAD) chain acyl-CoA dehydrogenases, respectively. The catalytic residue E376, identified in MCAD by chemical labeling studies (Powell & Thorpe, 1988) and confirmed by site-directed mutagenesis (Bross et al., 1990) and X-ray crystallography (Kim et al., 1993), is conserved in BCAD (E367 in the BCAD sequence). The corresponding glutamate residue is covalently modified by 2-pentynoyl-CoA in pig liver SCAD (Lundberg & Thorpe, 1993). On the basis of the rate of flavin bleaching by the substrate, the E367Q mutant BCAD expressed in *Escherichia coli* exhibits only 0.03% activity compared to that of the expressed wild type enzyme (Becker et al., 1993). Due to its high similarity to the mammalian enzymes and its ability to be purified in high yield from bacterial cells, a number of enzymatic studies have been performed with BCAD.

However, unlike the mammalian counterparts, BCAD reacts rapidly with oxygen. Upon reduction by the substrate,

[†] This research was supported by Research Grants GM29076 (J.J.P.K.), GM29344 (M.T.S.), and RR07198 (J.J.P.K.) from the National Institutes of Health. X-ray data were collected in part at the Resource for Protein Crystallography at the University of California-San Diego which is funded by Grant RR01644 from the National Institutes of Health.

[‡] Atomic coordinates have been deposited in the Brookhaven Protein Data Bank, entry 1BUC.

* To whom correspondence should be addressed.

[§] Medical College of Wisconsin.

[∥] University of Minnesota.

[⊗] Abstract published in *Advance ACS Abstracts,* February 1, 1995.

[1] Abbreviations: BCAD, butyryl-CoA dehydrogenase (also known as *Megasphaera elsdenii* short chain acyl-CoA dehydrogenase); FAD, flavin adenine dinucleotide; CoA, coenzyme A; MCAD, medium chain acyl-CoA dehydrogenase; SCAD, short chain acyl-CoA dehydrogenase; PC, Patterson correlation refinement; SA, simulated annealing; $NADP^+$, nicotinamide adenine dinucleotide phosphate.

0006-2960/95/0434-2163$09.00/0

mitochondrial acyl-CoA dehydrogenases undergo a very slow reaction with molecular oxygen. Reoxidation of reduced flavin of BCAD, however, is instantaneous as compared to hours required for the mitochondrial acyl-CoA dehydrogenases (Engel, 1981).

The three-dimensional structure of MCAD from pig liver mitochondria has been solved in its native and octanoyl-CoA-bound forms (Kim et al., 1993). We report here the X-ray structure of butyryl-CoA dehydrogenase from *M. elsdenii* determined at 2.5 Å resolution by the molecular replacement method. The structural investigation of BCAD was conducted with primarily two objectives: to gain an insight into the substrate specificity of fatty acyl-CoA dehydrogenases and to elucidate the structural basis for the distinctly high oxygen reactivity of the bacterial enzyme compared to the enzymes from mammalian mitochondria. The overall polypeptide folds of mammalian MCAD and bacterial BCAD are rather similar. A close comparison between the two structures, however, reveals subtle differences, including a single residue insertion in BCAD, that contribute to the distinct substrate specificities exhibited by these two enzymes. These differences could not be deduced from the primary sequence alignment which subsequently had to be corrected on the basis of the X-ray structures. In addition, the X-ray structure provides an interpretation for the oxygen reactivity.

MATERIALS AND METHODS

Crystallization. BCAD was isolated from *M. elsdenii* by the method of Engel (Engel, 1981) with the previously described modifications (Fink et al., 1986). The procedure involves four steps: acid treatment, ion exchange chromatography, salt fractionation, and gel filtration. The removal of CoA persulfide was carried out by dialysis against 10 mM dithionite followed by passage through the thiopropyl Sepharose column (Williamson & Engel, 1982; Fink et al., 1986). BCAD was crystallized in the presence of an equimolar amount of a dead-end inhibitor, acetoacetyl-CoA. Binding of acetoacetyl-CoA to the active site results in the appearance of a 580 nm absorbance band due to the formation of the charge-transfer complex, accompanied by a color change from yellow to brown-green. Crystallization was performed using the hanging- or sitting-drop methods (McPherson, 1985). The crystallization solution consisted of 120 mM potassium phosphate, pH 6.0, 60 mM Bis-Tris acetate, pH 6.0, 190 mM ammonium sulfate, and 4.3% poly(ethylene glycol) (PEG 4500, Dow Chemical). Crystallization drops, formed by mixing in 1.5:1.0 volume ratio of the acetoacetyl-CoA-bound BCAD (20 mg/mL) and the crystallization solution, respectively, were equilibrated by vapor diffusion against 50% PEG 4500. Crystallization was initiated at 19 °C, and full grown crystals were stored at 4 °C.

Preliminary X-ray Studies and Data Collection. Crystallization conditions were reproducible in yielding crystals with 0.2−0.5 mm in the longest dimension. The crystal growth was preceded by a phase separation. The crystals diffracted well to 2.4 Å resolution and lasted in the X-ray beam for about 20 h without significant decay. The space group determined from precession photographs and intensity data is $P422$ with unit cell dimensions $a = b = 107.8$ Å and $c = 153.7$ Å. Based on the assumption of one dimer per asymmetric unit, the calculated V_m value is 2.6 Å^3/Da which is well within the range for the average protein crystals (Matthews, 1968).

Table 1: Data Collection[a]

parameter	data set I	data set II	data set III
resolution (Å)	3.0	2.6	2.5
unique reflections (no.)	16 346	26 042	25 601
observations (no.)	77 242	102 444	81 262
completed (%)	87	94	80
R-sym* (%)	11.1	9.5	8.0
unit cell dimensions			
$a = b$ (Å)	108.1	108.1	107.8
c (Å)	154.0	154.1	153.7

[a]Data sets I and II were collected using a multiwire detector system at the University California-San Diego. Set III was collected with an *R*-axis II image plate system. All the crystals were cocrystallized with acetoacetyl-CoA. *R*-sym* = $\Sigma|I - \langle I\rangle|/\Sigma\langle I\rangle$ summed over all observations of all reflections.

Three intensity data sets were collected, two on the University of California-San Diego multiwire detector system, MARK III, and one on an *R*-axis II image plate detector system. Statistics on all three data sets are given in Table 1. A molecular replacement solution was derived with data set I, and the structure was partially refined with data set II and completed using data set III. Discrepancy between sets II and III was 13% (merging *R*-factor based on F^2) for 20 945 overlapping reflections. Detailed statistics on the different data sets are given in Table 1.

Structure Determination. The structure of BCAD was solved by the molecular replacement method (Rossman & Blow, 1962) using the X-PLOR computer program (Brünger et al., 1987). BCAD shares 40% amino acid sequence identity with pig liver MCAD. The refined crystal structure of native MCAD was used to construct the initial search model that was used throughout the molecular replacement studies. Using the TURBO (Roussel & Inisan, 1992) software on an Iris Silicon Graphics workstation, most of the MCAD residues were replaced with those corresponding to the BCAD sequence. Forty residues whose side chains in BCAD were larger than the side chains in MCAD and whose conformations could not be assigned without bias were modeled as alanines. The loop between MCAD residues 183 and 187 was manually shortened since these three residues are absent in the BCAD sequence, and the three insertions apparent in the sequence alignment were not constructed. The molecule of MCAD has 222 symmetry forming three distinct sets of dimers along the three perpendicular 2-fold axes (Kim et al., 1993). Throughout the text, the following nomenclature is used for identification of the dimers within the tetrameric molecule: the subunits from the tetramer are named as A, B, C, and D; the corresponding names for the dimers are AB(and CD), AC(BD), and AD(BC). In the structure of MCAD, an AB dimer constitutes the asymmetric unit, and both FAD and the substrate are bound at the interface of A and B monomers. There are few inter-subunit contacts within the AD or BC dimer.

(1) Rotation Search. Using data set I, three cross-rotation searches were performed: two with the MCAD-like dimer (dimer AB) as a probe in two different starting orientations and positions and one with a monomer as a probe. Rotation searches were carried out using the Patterson search proce-

dure in X-PLOR. Dimensions for the artificial cell that was searched were $a = b = 180$ Å and $c = 200$ Å. The angular search interval was set to 1.5°. The 7387 reflections greater than 2σ in the resolution range of 10−4 Å were used. The solutions from these three searches were very similar after Patterson correlation refinements. The final results of the rotation−translation search indicated that the asymmetric unit of BCAD consists of the AC dimer. After data set III was obtained, rotation and translation functions were recalculated with the correct dimer, AC. The cross-rotation search was performed with dimer AC as the probe and with 7578 reflections from data set III in the resolution range 15−4 Å. Patterson correlation refinement (PC) of the peaks from the rotation function solution was then performed. The minimization was carried out against a target function as defined by Brünger et al. (1990) and as implemented in the X-PLOR mannual.

(2) Translation Search. The translation search employed the standard linear correlation coefficient between the normalized, observed structure factors and the normalized, calculated structure factors. X-ray diffraction data between 15 and 4 Å resolution (data set I initially and set II subsequently) were used. Several translation searches were carried out using the search molecule oriented by the rotation function and refined by the PC method. The searches were performed in the range $x = 0-0.7$, $y = 0-0.7$, and $z = 0-1.0$, with sampling intervals between 5 and 1 Å.

(3) Self-Rotation Function. A self-rotation function was calculated in the resolution range of 15−4 Å. The maximum Patterson vector to be searched was set to 45 Å and the spherical polar angular grid to 1.5°. The highest 6000 peaks of the rotation function were included in the cluster analysis.

Structure Refinement. The refinement was carried out using X-PLOR. A rigid body minimization was followed by the Powell positional refinement followed by molecular dynamics refinement with a fast heat/cool procedure at 2000 and 300 K. Finally, an additional 120 steps of positional refinement were carried out at which point a $2|F_o| - |F_c|$ electron density map was calculated. Manual fitting and rebuilding of the model was carried out on an IRIS Silicon Graphics workstation using the TURBO software. Subsequent cycles of the refinement did not include a rigid body protocol except for the first refinement after the model of acetoacetyl-CoA was incorporated, and the fast heat/cool procedure was replaced by a slow-cool simulated annealing (SA) protocol. The slow-cool SA procedures were carried out starting at 3000 K at the beginning stages of the refinement and at 2000 K at the later stages with a time step of 0.5 fs. For calculations of omit maps, SA refinement was performed starting at 1000 K and a time step of 1 fs. The X-ray portion of the X-PLOR function was included with 100% of the weight calculated by the CHECK procedure of X-PLOR, at the earlier stages, and then lowered to 60−40% at the later refinement stages, in order to maintain good stereochemistry of the molecule. Noncrystallographic symmetry constraints were employed only in several of the earlier cycles, after which both monomers of the asymmetric unit were treated independently. The last few cycles of the refinement using data set III included temperature factor refinements following the end of each Powell minimization. Two rounds of grouped temperature factors preceded refinement of the individual temperature factors. All refinements and calculations were carried out on an IRIS Silicon Graphics workstation.

Table 2: Molecular Orientation in the Unit Cell (AB Dimer; Data Set I)

peak index	before PC refinement			after PC refinement			rotation function	Patterson correlation
	θ_1	θ_2	θ_3	θ_1	θ_2	θ_3		
26	155.7	45.0	72.4	144.7	39.2	95.7	1.567	0.0615
36	152.7	42.5	90.4	144.7	39.2	95.6	1.523	0.0615
51	132.4	35.0	106.7	144.7	39.2	95.7	1.475	0.0612

RESULTS

Molecular Replacement. The initial molecular replacement calculations were carried out using data set I. The results of the rotational searches performed with the dimers in two different starting orientations were very similar, and therefore the results from only the second search are shown. The 100 highest peaks were chosen for further study in the PC refinement. Three strong peaks emerged after the PC refinement, all of which converged to approximately the same orientation. The values of the three peaks before and after the PC refinement are given in Table 2. When the rotation search was performed using a monomer, a single peak with the highest correlation factor after the PC refiniment was identified. The Eulerian angles (148.3°, 40.2°, 90.4°) were consistent with those obtained from the searches with a dimer. Several translation searches were carried out to find the molecular position of the AB dimer probe in the unit cell. All of the resulting positions were located on or near a crystallographic 2-fold axis, thus producing large overlaps with symmetry related molecules. A self-rotation function contained, in addition to the crystallographic symmetry element, only a peak close to the y axis at $\psi = 5.3°$ and $\phi = 0°$. This noncrystallographic 2-fold axis is located in the xy plane, perpendicular to the crystallographic 2-fold axis around which the solutions from the translation searches were positioned. This observation suggested that the relationship between the subunits A and B of the ABCD tetramer in the crystal of BCAD is defined by the crystallographic 2-fold axis and that the asymmetric unit is built from the subunits A and C related by the noncrystallographic 2-fold symmetry at $\psi = 5.3°$ and $\phi = 0°$. This local 2-fold axis, in combination with the crystallographic axis that is parallel to z at $x(y) = 0.5$, generates the tetramer with 222 symmetry. The location of the noncrystallographic symmetry axis in the z direction was determined from the translation searches. Although the results of the translation searches using dimer AB contained large overlaps in the xy direction, they did not overlap in the z direction. When the tetramer was generated at the position coresponding to the results of the dimer translation search, the center of the tetrameric molecule was at $z = 0.75$. The position of the asymmetric unit in the $z = 0.75$ plane is shown in Figure 1. The refinement was carried out starting from the dimer AC oriented as shown in Figure 1.

Refinement of the Molecular Replacement Solution. The molecular replacement solution was improved by a rigid body refinement with the X-PLOR program using reflections in the 10−3 Å resolution range. At this stage the R-factor was 49.9%. The Powell positional refinement lowered the R-factor to 37.9%, eliminating a large number of bad contacts

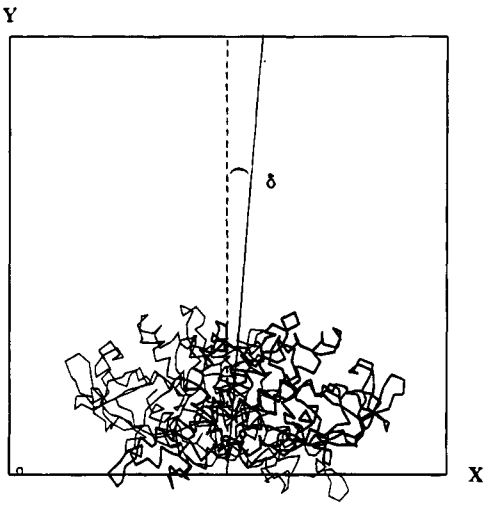

FIGURE 1: Orientation of the BCAD dimer in the *xy* plane of the unit cell. In the refined structure, the local 2-fold axis is inclined by $\delta = 3.8°$ away from the y axis. One monomer is drawn in thick lines and the other in thin lines.

Table 3: Refinement of BCAD by X-PLOR

data set	rounds of simulated annealing	resolution (Å)	reflections (no.)	R_{start}	R_{end}	atoms in last cycle (no.)
I	1–5[a]	10.0–3.0	15 342	0.379	0.265	5886
II	6–18	8.0–2.6	23 080	0.275	0.239	5924
III	19–20[b]	8.0–2.4	26 003	0.258	0.226	5924
III	21–22[c]	8.0–2.4	26 003	0.226	0.212	5924
III	23–28[d]	8.0–2.4	26 003	0.222	0.193	6032

[a]Prior to the first cycle of simulated annealing, 40 steps of Powell minimization lowered the *R*-factor from 0.499 to 0.379. [b]During cycles 19 and 20, a single insertion in helix E was made and the side chains were corrected. [c]Helix F and the extended loop connecting helices C and D were corrected in cycles 21 and 22. [d]Starting with cycle 23, a model of acetoacetyl-CoA was included. The stereochemistry was optimized in the last stage of refinement, and *B*-factors were refined at the end of each cycle.

within the constructed dimer. One cycle of the molecular dynamics refinement with a fast heat/cool procedure at 2000/300 K, followed by 120 steps of positional refinement, lowered the *R*-factor to 27.7%. The $2|F_o| - |F_c|$ electron density map calculated with this model was interpretable, and it showed that the majority of the model fits well within the density. There were several regions of disconnected density. Several cycles of SA interrupted by model rebuilding were needed to introduce all of the correct side chains. The refinement was continued with data set II with 18 cycles of SA, and the refinement was completed with 10 more cycles using data set III. The regions that were originally unclear and appeared disordered were well defined in the omit maps using data set III, and consequently a complete model of BCAD was successfully built and refined. In addition to $2|F_o| - |F_c|$ maps, the electron density maps with omitted portions of the input model were also calculated ($2|F_o| - |F_c|$ omit maps) in order to confirm the backbone positions and side chain assignments. Data set III was also used to build the model of acetoacetyl-CoA in the active site of BCAD. A summary of the refinement progress is given in Table 3.

The refined BCAD structure has an *R*-factor of 19.3% when all of the observed X-ray data (26 003 reflections) between 8.0 and 2.4 Å are included. The final refined model

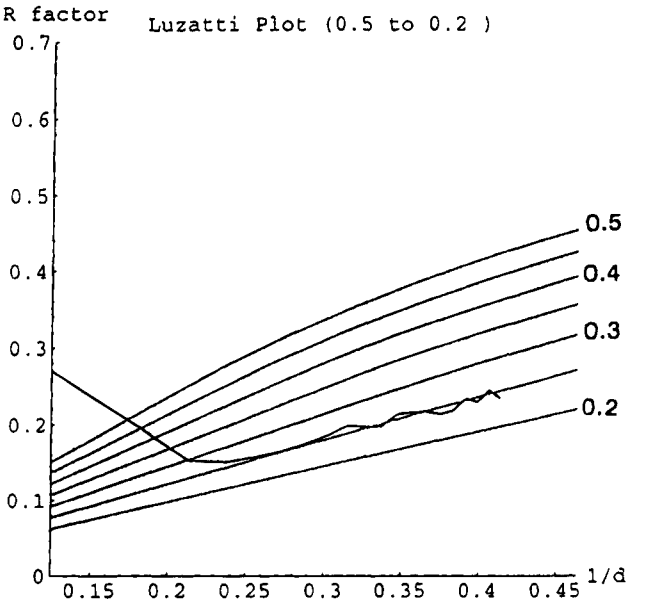

FIGURE 2: Theoretical estimates of the rms positional errors in the atomic coordinates of BCAD according to Luzzati (1952). The upper limit coordinate mean error estimated from this plot is 0.3 Å.

of the BCAD–acetoacetyl-CoA complex contains 6032 non-hydrogen atoms; water molecules are not included.

The root mean square (rms) deviations of bond lengths and bond angles are 0.010 Å and 2.7°, respectively. By the method of Luzzati (1952), the upper limit error of the refined BCAD coordinates is estimated to be 0.3 Å (Figure 2). The average temperature factor for all atoms is 18 Å^2. The rms deviation of the backbone atoms between the two monomers in the asymmetric unit is 0.33 Å which is within the experimental error, indicating that the two monomer structures are essentially identical in the crystalline state. Therefore, only the monomer A structure will be described unless indicated. The local symmetry axis in the final refined structure is 3.8° away from the $y(x)$ axis.

Description of the Structure. A Ramachandran plot of the main chain dihedral angles, ϕ and ψ, showed that there were five non-glycine residues/monomer with positive ϕ angles. Two of these residues are E367, the catalytic base in the active site, and F160 at the *si*-face of the isoalloxazine ring of the FAD molecule. The other three residues are N163, also on the *si*-face of the FAD, D220, a part of a β-bulge formation, and F275, at the interface of the two monomers (monomers A and B). E376, the catalytic base in MCAD, also has similar Ramachandran values.

The overall folding of BCAD is rather similar to that of MCAD. The monomer consists of three domains: two α-helical domains at the N- and C-terminal regions and the β-sheet domain in the middle. The FAD is located between the β-domain and the C-terminal domain of one subunit and the C-terminal domain of a neighboring subunit. In the crystals of BCAD, the two subunits involved in the binding of the flavin are related by a crystallographic 2-fold symmetry. A ribbon diagram of a monomer of BCAD is shown in Figure 3. The FAD and acetoacetyl-CoA molecules are represented with ball–and–stick models. All the α-helices and β-sheets are labeled according to the scheme used in MCAD (Kim et al., 1993).

The Active Site. A $2|F_o| - |F_c|$ map, calculated with the refined protein atoms and data set III, yielded well-defined

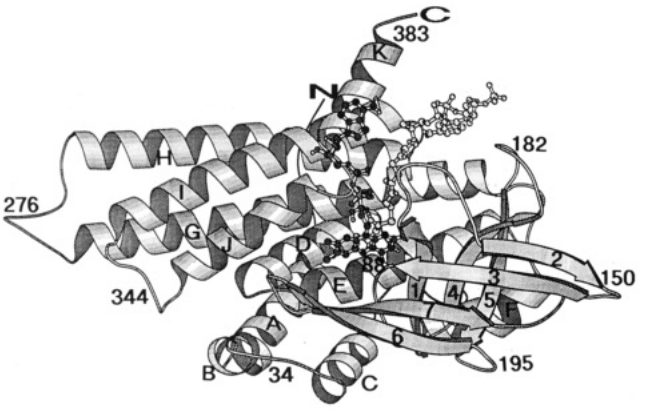

FIGURE 3: Ribbon diagram of a monomer of butyryl-CoA dehydrogenase in the presence of acetoacetyl-CoA. The FAD is represented by solid balls, and the acetoacetyl-CoA is represented by open balls. N- and C-terminal ends are indicated. The α-helices are labeled in alphabetical order, and β-strands are in numerical order from N- to C-terminal end. The figure was drawn by using the program MOLSCRIPT (Kraulis, 1991).

densities in the active site close to the FAD. The densities were easily interpreted as the bound inhibitor, acetoacetyl-CoA. Figure 4 depicts the model of acetoacetyl-CoA in the final $2|F_o| - |F_c|$ electron density map. Acetoacetyl-CoA is bound in the active site of BCAD between helices E and G (Figures 3 and 8). The overall shape of the enzyme-bound inhibitor resembles that of the octanoyl-CoA bound to the active site of MCAD (Kim et al., 1993). The plane of the acetoacetyl portion of the substrate is parallel to and located at the *re*-face of the isoalloxazine ring of the FAD. The plane of the terminal methyl and carbonyl groups of the acetoacetate is almost perpendicular to the phenolic ring of Y366. The carbonyl oxygen of the thioester is hydrogen bonded to ribityl 2′-OH of the FAD and the main chain amide nitrogen of E367 as observed in the structure of MCAD complexed with octanoyl-CoA. The coenzyme A portion of the inhibitor is bound inside a crevice that is lined by mostly conserved residues (Figure 5). Among the residues previously identified to be in the CoA binding site of MCAD (Kim et al., 1993), the only differences are T135 and L243 in BCAD, instead of S142 and F252 in MCAD, respectively, in the vicinity of the pantothenate unit of the CoA; S191 of MCAD that forms a weak hydrogen bond with the 3′-phosphate of the adenosine is replaced by N182 in BCAD. Hydrogen bonding interactions of the pantothenic acid with the protein side chains are somewhat different in BCAD compared to MCAD. The two carbonyl groups of the pantothenate are hydrogen bonded to R247, whereas in the structure of MCAD, only one of the carbonyl oxygen groups makes a direct hydrogen bond with R256 and the other one is bonded to a water molecule. This difference, a stronger interaction between the polypeptide and the pantothenate moiety, might be partly responsible for the thighter binding of CoA persulfide to BCAD than to MCAD.

The active site residues E367 and Y366 found in the structure of the complex between BCAD and acetoacetyl-CoA are in the same conformation as E376 and Y375 in octanoyl-CoA-bound MCAD, respectively. The residues around the Cα−Cβ bond and the FAD in BCAD align almost perfectly (rms = 0.2 Å) with the corresponding residues of MCAD (Figures 6 and 9), despite the fact that other parts of the molecule exhibit significant differences. This confirms that the active site arrangement found in BCAD and MCAD structures is the optimal one to carry out the catalysis.

FAD has an extended conformation as it was observed in MCAD. A structural comparison clearly shows that most of the residues in the FAD environment are identical in BCAD and MCAD (Figure 6). A major difference is that W166 of MCAD is replaced by F160 in BCAD.

DISCUSSION

Interpretation of the structures of homologous enzymes is largely based upon their differences as well as their similarities. The existing amino acid differences are naturally occurring "mutants" pointing to possible residues linked to the particular enzymatic properties. In addition, conserved residues help to identify key factors in catalytic reactions and in construction of the overall protein topology.

Comparison with MCAD. There are 39% and 44% amino acid sequence identities between BCAD and human liver

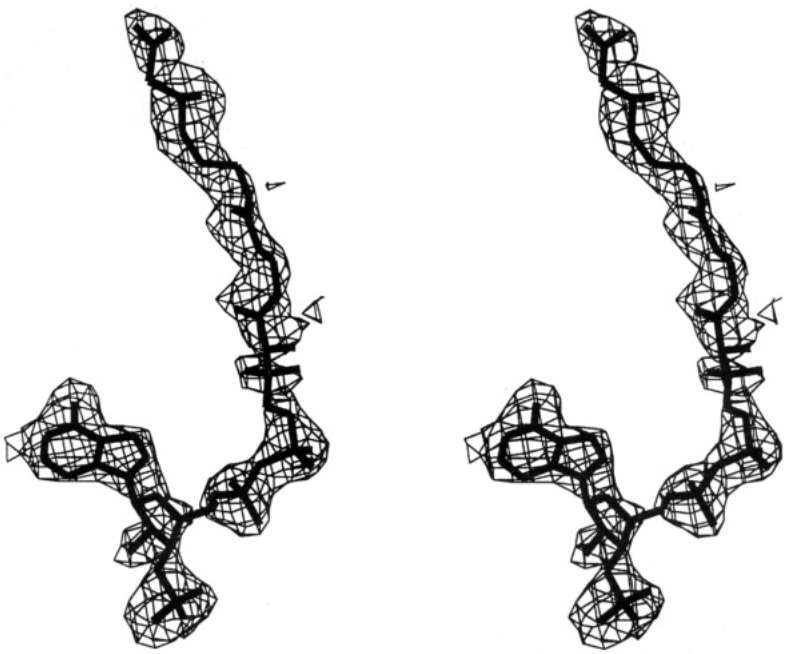

FIGURE 4: Model of acetoacetyl-CoA fitted in the final $2|F_o| - |F_c|$ electron density map. The map was contoured at 1.0σ level.

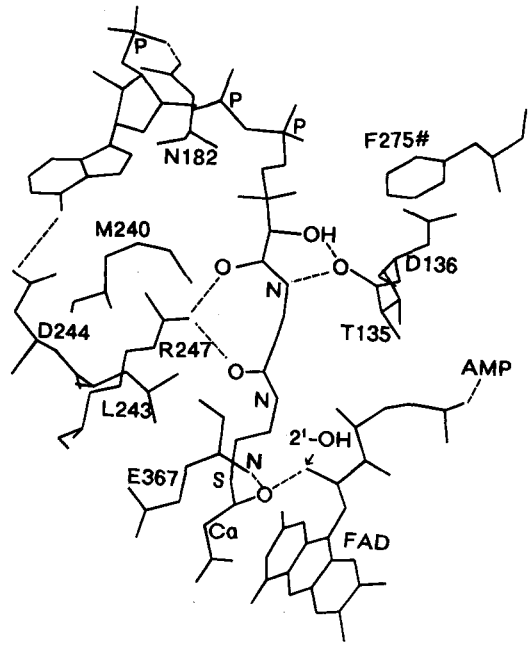

FIGURE 5: Residues lining the acetoacetyl-CoA binding cavity. Possible hydrogen bonds are shown by dashed lines. F275# belongs to the neighboring subunit. Position of the Cα of the acetoacetate and the position of 2′-OH of the ribose portion of FAD are also indicated.

MCAD and between BCAD and human SCAD, respectively. In both BCAD and SCAD, the surface loop connecting β-strands 4 and 5 (Figure 3) is shorter by three residues than in MCAD. In the structure of MCAD, this loop is at the entrance point of the substrate into the active site cavity, near the binding site of the adenosine moiety of the CoA. Temperature factors for this region are relatively high (30–40 Å^2) indicating that the loop is flexible and probably of no crucial structural importance. In the BCAD sequence, a total of five residues are inserted in three positions of the primary sequence of MCAD. Residues from 66 through 68 are a part of the long and extended surface loop connecting helices C and D. Residue 150 belongs to the connecting turn between the β-strands 2 and 3, and the insertion of this residue does not cause any perturbation in the structure. The third insertion falls within helix E, and this is of particular structural significance. The rms deviations of the backbone atoms (excluding BCAD residues 50–100 and the corresponding MCAD residues) of the two proteins are 1.26 and 1.19 Å for the native and octanoyl-CoA-bound form of MCAD, respectively.

Sequence comparison programs, such as Bestfit (Smith & Waterman, 1981) and Gap (Needleman & Wunsch, 1970), align the sequences of BCAD and MCAD such that one residue is inserted in the BCAD sequence at the end of the helix D. The insertion of one residue would disrupt the helical configuration. In the initial model, the insertion was made at this position; however, the model did not fit well into the electron density after the refinement. The electron density in this region was poorly defined and contained interruptions, and the shape of the side chains was unclear. Omit maps did not help in solving the problem until data set III was obtained. A $2|F_o| - |F_c|$ map clearly showed that the insertion was out of place, and in addition, there was a frame shift by one residue in the side chain assignments within helix E. A careful examination of the electron density map, the side chain positions, and the overall secondary structure revealed that one residue is inserted in the third turn of helix E after residue 93 (N101 in MCAD). In the structure of MCAD, this helical turn contains only three residues (3_{10} helix) so that insertion of the additional residue should in fact restore the regular helical arrangement. However, the proline residue at position 100 in BCAD induces a large kink and disrupts the regular hydrogen bonding pattern. Figure 7 shows the sequence alignment of the residues within helices D and E of MCAD and BCAD based on the X-ray structures of the two enzymes.

Substrate Specificity. A significant discrepancy between the structures of BCAD and MCAD is exhibited in the "bottom" of the fatty acid binding pocket. The acyl-CoA

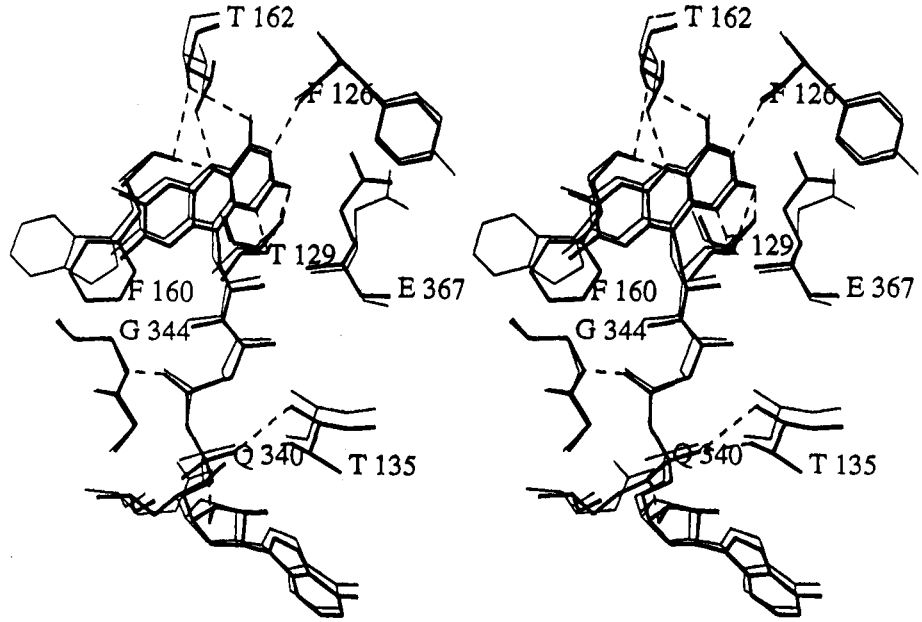

FIGURE 6: Stereoview of the residues near the FAD binding site. BCAD residues are drawn in thick lines. Residues represented by thin lines are from the structure of MCAD complexed with octanoyl-CoA (Kim et al., 1993). The numbers correspond to the sequence of BCAD. Hydrogen bonds are shown as dashed lines.

```
            80          90          100         109
            |           |           |           |
PMCAD  ....SCLITEELAYGCTGVQTAIEAN-TLGQVPLI....
HMCAD  ....ACLISEELAYGCTGVQTAIEGN-SLGQMPII....
RMCAD  ....ACLITEELAYGCTGVQTAIEAN-SLGQMPVI....
HSCAD  ....YAIAMEEISRGCASTGVIMSVNNSLYLGPIL....
RSCAD  ....YSIALEEISRGCASTGVIMSVNNSLYLGPIL....
 BCAD  ....YILAVEELAKYDAGVAITLSATVSLCANPIW....
            |           |           |           |
           72          82          92          102
```

FIGURE 7: Portion of a sequence alignment of pig MCAD, human MCAD, rat MCAD, human SCAD, rat SCAD, and BCAD. The alignment was made on the basis of the structural homology between pig MCAD and BCAD. The numbers above the sequences correspond to the MCAD sequence, and the numbers below the sequences correspond to BCAD and SCADs. There is a single residue insertion in the middle of helix E in BCAD and SCAD.

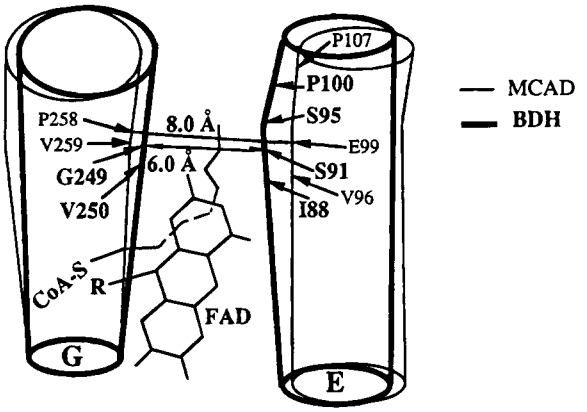

FIGURE 8: Schematic presentation of the helices E and G in the structures of MCAD (thin lines) and BCAD (thick lines). Positions of the residues involved in the substrate recognition and in determining the conformations of the helices are labeled by arrows and numbers. Distance between Cα atoms of G249 and S91 in BSCAD is 6.0 Å, and the corresponding distance in MCAD (between P258 and E99) is 8.0 Å. The structures of FAD and octanoyl-CoA in the active site are also shown in a simplified fashion.

substrate binds between helices E and G. In BCAD, these two helices are much closer than those in MCAD (Figure 8). The distance between the Cα atoms of I88 and V250 in BCAD is 7.4 Å compared to 8.6 Å between the Cα atoms of the corresponding T96 and V259 in MCAD. Similarly, the S91 to G249 distance is 6.0 Å in BCAD compared to 8.0 Å between E99 and P258 in MCAD. Clearly, the binding cavity of BCAD is much smaller. There are two reasons for the smaller distance between helices E and G in the substrate binding cavity of BCAD compared to the corresponding distance in MCAD: (a) a single residue insertion in the middle of helix E bends and distorts this helix bringing it closer to the substrate; (b) in BCAD and SCAD there is no proline in helix G corresponding to P257 of MCAD, so that overall the helix in BCAD is straighter and closer to the substrate by approximately 0.5−0.7 Å. P257 is conserved among MCAD enzymes from pig, human, and rat mitochondria. In pig MCAD, residue 258 is also a proline.

The model of octanoyl-CoA from Kim et al. (1993) was overlaid on the structure of BCAD based on the best fit of the main chain atoms of MCAD and BCAD (Figure 9). If the octanoyl-CoA binds BCAD, the side chain of BCAD, I88, would be too close to C_6, C_7, and C_8 atoms of octanoyl-CoA (1.6, 0.7, and 1.3 Å, respectively). Even if the conformation of I88 were different, other residues in the binding cavity would prevent binding of a longer fatty acyl chain. For example, A92 and L96 on one side of the bottom of the cavity and a hydrogen bond between Y366 and Q253 on the other side do not allow binding of the substrate in either of these directions. In the active site, the C_2-C_3 bond of the acetoacetyl-CoA is "sandwiched" very tightly betweeen the isoalloxazine ring of the FAD and the carboxylate of E367, as was previously observed in the structure of the MCAD complexed with octanoyl-CoA. BCAD exhibits none or very low activity with the 2- or 3-methylacyl-CoA substrates (Williamson & Engel, 1984). Introduction of a methyl group at either C_2 or C_3 position would disturb the proper binding and orientation of the substrate. The 4-methylpentanoyl-CoA, however, is a relatively good substrate, and the structure of the BCAD active site has enough space to accept this branched chain acyl-CoA. All of the residues discussed above as being involved in the substrate recognition are identical to or homologous in mitochondrial SCAD. Residues I88, S91, G249, V250, and Q253 in BCAD correspond to V, S, G, I, and Q, respectively, in rat and human SCAD. From the amino acid sequences of rat and human SCAD, it is evident that these enzymes also contain an additional residue (N94) in helix E inserted probably at the same position as observed in BCAD.

The three-dimensional structure of BCAD reveals that the weak sequence homology within helices D and E among different acyl-CoA dehydrogenases is a determining factor in substrate specificity. The primary structure was insufficient to determine the residues involved in substrate recognition. The insertion of a single residue causes a shift in the amino acid sequence of the helix. Thus, the position of the insertion defines which side chains are oriented toward the substrate.

From this work, it is not clear why BCAD isolated from *M. elsdenii* contains tightly bound CoA persulfide ($CoASS^-$). The binding of $CoASS^-$ at the active site near flavin produces a charge-transfer band which is responsible for the green color (Williamson et al., 1982). Why does BCAD bind $CoASS^-$ more tightly than MCAD does? The following two explanations are possible. (1) The total binding energy of butyryl-CoA to BCAD is approximately the same as that of octanoyl-CoA to MCAD, since the respective K_m values are essentially the same ($\sim 10^{-6}$ M). Therefore, although it is not obvious from the current structure, the substrate binding energy contributed from the CoA moiety of the substrate in BCAD must be larger than the corresponding energy found in MCAD, since the hydrophobic interactions involving a four-carbon alkyl chain (butyryl-CoA) with BCAD is smaller than those involving an eight-carbon alkyl chain (ocanoyl-CoA) with MCAD. Since the CoA persulfide does not have any alkyl chain for the hydrophobic interactions, it would bind to BCAD more tightly than to MCAD. Detailed binding energy calculations and/or measurements for the two enzymes will be able to confirm this explanation. (2) Because the persulfide has a negative charge, it may have a higher probability of binding to acyl-CoA dehydrogenases with an active site that has a slight positive charge, which in turn means a more positive redox potential (easier electron transfer to the flavin). A comparison of active site residues between the two enzymes reveals that a negatively charged residue (E99) is located at the bottom of the active site cavity in MCAD, whereas the corresponding residue in BCAD (also both rat and human SCAD) is a neutral residue (S91). This explanation is supported by the measured redox potentials because the redox potential of BCAD, which forms a tight

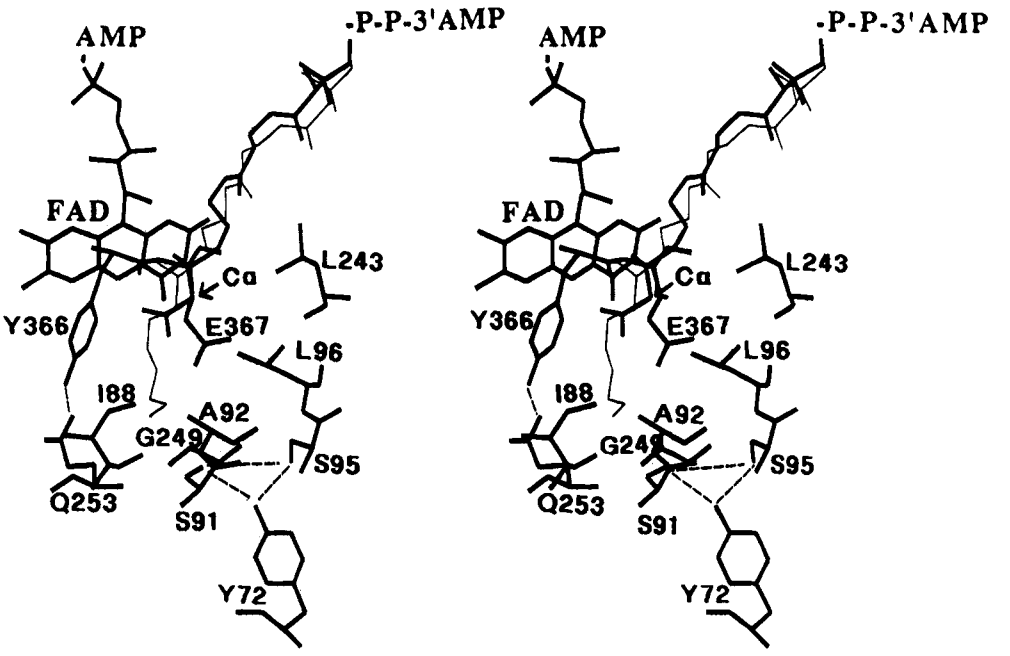

FIGURE 9: Stereodrawing of BCAD active site. Octanoyl-CoA from the MCAD−C_8-CoA complex is overlaid onto the BCAD structure and represented by a thin line. Hydrogen bonds are shown as dashed lines.

complex with persulfide, is significantly more positive (−79 mV) (Fink et al., 1986) than the redox potential of MCAD (−145 mV) (Gustafson et al.,1986; Lenn et al., 1990) which does not form the green complex to as great an extent. This idea of the magnitude of the binding constant of a negatively charged ligand being correlated to redox potential is supported by the linear correlation of the binding of bisulfite (HSO_3^-) to free flavin (Muller & Massey, 1969) and flavoprotein oxidase enzymes (Massey et al., 1969). The more positive the redox potential of the free flavin or flavoprotein oxidases, the tighter the binding of the bisulfite. The positive potential of the free flavins was caused by electron-withdrawing groups at the C_7 or C_8 positions of the flavin ring, and the positive charges on the flavoprotein oxidases were caused by the positively charged amino acid sidechains near the N_1 position of the flavin ring (Ghisla & Massey, 1990). As the redox potentials and structures of other acyl-CoA dehydrogenases become available, we will further explore this proposed correlation.

Oxygen Reactivity. Why is the flavin of butyryl-CoA dehydrogenase from *M. elsdenii* prone to a rapid reoxidation by molecular oxygen? This question can be answered by first examining the factors influencing a slow reoxidation of the reduced FAD by molecular oxygen in the mammalian enzymes. Wang and Thorpe (1991) have determined that the binding of different acyl-CoA analogs to the active site of photochemically reduced MCAD increases the half-life of the reduced FAD up to 3500-fold. The extent of the effect was dependent on the presence of a thioester carbonyl group, which also affected the dissociation constants of the substrate analogs. The crystal structures of octanoyl-CoA-bound MCAD and acetoacetyl-CoA-bound BCAD determined that the carbonyl oxygen of the thioester is crucial in binding of the substrates. Kim et al. (1993) have also shown that the ordered water molecules in the active site of the native MCAD are displaced by the carbon atoms of the bound fatty acid. This observation is in agreement with the mechanism proposed by Wang and Thorpe. They have suggested that the strong suppression of oxygen reactivity observed with certain ligands reflected desolvation of the active site and subsequent destabilization of the superoxide anion intermediate formed during reoxidation of flavin. The redox potential for the reduction of molecular oxygen is strongly solvent dependent (Sawyer & Nanni, 1981). In addition, model studies showed large decreases in the reactivity of dihydroflavins toward molecular oxygen in an apolar solvent (Müller et al., 1975). The reduction of oxygen within a protein matrix that is unable to effectively solvate the superoxide anion is likely to be thermodynamically unfavored. The three-dimensional structure of MCAD confirmed that the FAD is buried within the protein molecule. The *re*-face of the flavin is protected upon substrate binding, whereas the *si*-face is covered by W166 and M165.

The isoalloxazine ring of the FAD in MCAD is covered by the amino acid side chains. In contrast, the dimethylbenzene ring of the FAD is exposed to solvent in the structure of BCAD. It is likely that electrons are transferred to electron-transfer flavoprotein through these two methyl groups, similar to the flavodoxins and the proposed mechanism involved in the ferredoxin-$NADP^+$ reductase family of enzymes (Karplus et al., 1991; Correll et al., 1992). The exposure of the FAD is primarily due to the substitution of F160 in BCAD for W166 in MCAD. In addition, the substitution of S348 in BCAD for N357 in MCAD contributes to the exposure of the flavin to the solvent. Furthermore, the interatomic distances between the residues of one to the other monomer at the dimer interface of the FAD binding site are somewhat longer (by 0.5−0.7 Å) in BCAD than in MCAD. We propose that oxidation of the reduced FAD molecule in BCAD by molecular oxygen is much more favored than in MCAD due to mainly a change in polarity of the flavin environment. In BCAD, the superoxide anion can be stabilized by solvation and yield the final product, H_2O_2. In MCAD, according to the mechanism proposed by Wang and Thorpe (1991), any superoxide formed is likely to return the electron to flavin faster than it could diffuse to the exterior of the protein.

The solvent accessible surface area of the FAD was examined in BCAD and MCAD in the presence and absence of acetoacetyl-CoA and octanoyl-CoA, respectively, using the Lee and Richards (1971) algorithm as implemented in X-PLOR. Most of the atoms in the adenosine moiety of the FAD, in all four cases, are exposed to the solvent. The ribityl atoms of the FAD are not accessible to solvent molecules in the presence of acetoacetyl-CoA. Most importantly, the C_8 of the isoalloxazine ring in BCAD is equally exposed to the solvent both in the presence and absence of acetoacetyl-CoA. This atom has an accessible surface area of 1.1 $Å^2$ which can be interpreted as a small solvent cavity that can accommodate one water molecule. In the MCAD structure, all atoms of the isoalloxazine ring are protected from the solvent in the presence of the substrate, whereas the atoms of the dimethylbenzene portion are protected from the solvent even in the absence of the substrate.

Rat liver acyl-CoA oxidase shares high sequence homology with mitochondrial acyl-CoA dehydrogenases. Interestingly, despite a significant sequence identity, the oxidase does not contain tryptophan at the position equivalent to W166 of MCAD. Acyl-CoA oxidase contains a threonine (Matsubara et al., 1989), a much smaller and more polar residue, thus supporting the hypothesis that flavin protection from the solvent determines the rate of reaction with molecular oxygen. In addition, the oxidase, like BCAD, also has a serine at the position equivalent to N357 of MCAD.

ACKNOWLEDGMENT

We thank Ming Wang for his assistance in the data collection and Sandro Ghisla for helpful discussions about the green enzyme.

REFERENCES

Baldwin, R. L., & Milligan, L. P. (1964) *Biochim. Biophys. Acta 92*, 421−432.
Becker, D. F., Fuchs, J. A., Banfield, D. K., Funk, W. D., Ross, T. A., MacGillivray, T. A., & Stankovich, M. T. (1993) *Biochemistry 32*, 10736−10742.
Beinert, H. (1963) in *The Enzymes 7*, (Boyer, P. D., Lardy, H., & Myrback, K., Eds.) pp 447−466, Academic, New York.
Bross, P., Engst, S., Strauss, A. W., Kelly, D. P., Rashed, I., & Ghisla, S. (1990) *J. Biol. Chem. 265*, 7116−7119.
Brünger, A. T., Kuriyan, J., & Karplus, M. (1987) *Science 235*, 458−460.
Brünger, A. T., Krukowski, A., & Erickson, M. (1990) *Acta Crystallogr. A46*, 585−593.
Correll, C. C., Batie, C. J., Ballou, D. P., & Ludwig, M. L. (1992) *Science 258*, 1604−1610.
Elsden, S. R., & Lewis, D. (1953) *Biochem. J. 55*, 183−189.
Engel, P. C. (1981) *Methods Enzymol. 71*, 359−366.
Fink, C. W., Stankovich, M. T., & Soltysik, S. (1986) *Biochemistry 25*, 6637−6643.
Ghisla S., & Massey, V. (1991) in *Chemistry and Biochemistry of Flavoenzymes* (Muller, F., Ed.) Vol. 2, pp 244−304, CRC Press, Baton Rouge, FL.
Gustafson W. G., Feinberg, B. A. & McFarland, J. T. (1986) *J. Biol. Chem. 261*, 7733−7741.
Hoskins, D. D. (1966) *J. Biol. Chem. 241*, 4472−4479.
Karplus, P. A., Daniels, M. J., & Herriott, J. R. (1991) *Science 251*, 60−66.
Kim, J.-J. P., Wang, M., & Paschke, R. (1993) *Proc. Natl. Acad. Sci. U.S.A. 90*, 7523−7527.
Kraulis, P. J. (1991) *J. Appl. Crystallogr. 24*, 946−950.
Lee, B., & Richards, F. M. (1971) *J. Mol. Biol. 55*, 379−400.
Lenn, N. D., Stankovich, M. T., & Liu, H. (1990) *Biochemistry 29*, 3709−3715.
Lundberg, N. N., & Thorpe, C. (1993) *Arch. Biochem. Biophys. 305*, 454−459.
Luzatti, P. V. (1952) *Acta. Crystallogr. 5*, 802−810.
Mahler, H. R. (1954) *J. Biol. Chem. 206*, 13−26.
Massey, V., Muller, F., Feldberg, R., Schuman, M, Sullivan, P. A., Howell, L. G., Mayhew, S. G., Matthews, R. G., & Foust, G. P. (1969) *J. Biol. Chem. 244*, 3999−4006.
Matsubara, V., Indo., Y., Naito, E., Ozasa, H., Glassberg, R., Vockley, J., Ikeda, Y., Kraus, J., & Tanaka, K. (1989) *J. Biol. Chem. 264*, 16321−16331.
Matthews, B. W. (1968) *J. Mol. Biol. 33*, 491−497.
McPherson, A. (1985) *Methods Enzymol. 114*, 112−128.
Müller, F., & Massey, V. (1969) *J. Biol. Chem. 244*, 4007−4016.
Müller, F., Jarbandhan, T., Gast, R., & Grande, H. J. (1975) in *Reactivity of Flavins* (Yagi, K., Ed.) pp 51−70, University of Tokyo Press, Tokyo.
Needleman, S. B., & Wunsch, C. D. (1970) *J. Mol. Biol. 48*, 443−453.
Powell, P. J., & Thorpe, C. (1988) *Biochemistry 27*, 8022−8028.
Rossman, M. G., & Blow, D. M. (1962) *Acta Crystallogr. 15*, 24−31.
Roussel, A., & Inisan, A. G. (1992) *TURBO-manual*, Bio-Graphics, Marseille, France.
Sawyer, D. T., & Nanni, E. J. (1981) in *Oxygen and Oxygen Radicals in Chemistry and Biology* (Rodgers, M. A. J., & Powers, Eds.) pp 15−44, Academic Press, New York.
Smith, T. F., & Waterman, M. S. (1981) *Adv. Appl. Math. 2*, 482−489.
Steyn-Parve, E. P., & Beinert, H. (1958) *J. Biol. Chem. 233*, 853−861.
Wang, R., & Thorpe, C. (1991) *Biochemistry 30*, 7895−7901.
Williamson, G., & Engel, P. C. (1982) *Biochim. Biophys. Acta 706*, 245−248.
Williamson, G., & Engel, P. C. (1984) *Biochem. J. 218*, 521−529.
Williamson, G., Engel, P., Mizzer, J. P., Thorpe, C, & Massey V. (1982) *J. Biol. Chem. 257*, 4314−4320.

BI941861L